Cellular structural biology as revealed by cryo-electron tomography

Irobalieva, Rossitza N ; Martins, Bruno ; Medalia, Ohad

Abstract: Understanding the function of cellular machines requires a thorough analysis of the structural elements that underline their function. Electron microscopy (EM) has been pivotal in providing information about cellular ultrastructure, as well as macromolecular organization. Biological materials can be physically fixed by vitrification and imaged with cryo-electron tomography (cryo-ET) in a close-to-native condition. Using this technique, one can acquire three-dimensional (3D) information about the macromolecular architecture of cells, depict unique cellular states and reconstruct molecular networks. Technical advances over the last few years, such as improved sample preparation and electron detection methods, have been instrumental in obtaining data with unprecedented structural details. This presents an exciting opportunity to explore the molecular architecture of both individual cells and multicellular organisms at nanometer to subnanometer resolution. In this Commentary, we focus on the recent developments and in situ applications of cryo-ET to cell and structural biology.

DOI: https://doi.org/10.1242/jcs.171967

© 2016. Published by The Company of Biologists Ltd | Journal of Cell Science (2016) 129, 469-476 doi:10.1242/jcs.171967

COMMENTARY

ARTICLE SERIES: IMAGING

Cellular structural biology as revealed by cryo-electron tomography

Rossitza N. Irobalieva[1], Bruno Martins[1] and Ohad Medalia[1,2,*]

ABSTRACT

Understanding the function of cellular machines requires a thorough analysis of the structural elements that underline their function. Electron microscopy (EM) has been pivotal in providing information about cellular ultrastructure, as well as macromolecular organization. Biological materials can be physically fixed by vitrification and imaged with cryo-electron tomography (cryo-ET) in a close-to-native condition. Using this technique, one can acquire three-dimensional (3D) information about the macromolecular architecture of cells, depict unique cellular states and reconstruct molecular networks. Technical advances over the last few years, such as improved sample preparation and electron detection methods, have been instrumental in obtaining data with unprecedented structural details. This presents an exciting opportunity to explore the molecular architecture of both individual cells and multicellular organisms at nanometer to subnanometer resolution. In this Commentary, we focus on the recent developments and *in situ* applications of cryo-ET to cell and structural biology.

KEY WORDS: Cryo-electron tomography, *In situ* structural determination, Macromolecular assemblies

Introduction

In cells, intricate ensembles and networks of molecular machines execute a multitude of specialized cellular tasks. Many of the components of these networks have been identified by proteomics (mainly mass spectrometry; Passarelli and Ewing, 2013). However, an immense amount of information is needed to decipher the structure of a myriad of molecular assemblies that comprise the crowded and complex environment of the cell. *In situ* structural information is especially crucial in resolving the *modus operandi* of these cellular entities.

Electron microscopy (EM) has long been the technique of choice for visualizing biological specimens and cellular structures. Back in 1934, Ladislaus Marton was the first to use EM for imaging a biological specimen – sundew plant tissue (Marton, 1934). Throughout the years, the development of fixation, embedding and sectioning protocols has allowed us to visualize and characterize various cellular components (McIntosh, 2007). Such tools help reveal the basic organization of cells and set the foundation for *in situ* structural biology. In the past couple of decades, technical developments in EM (Schröder, 2015), as well as specimen preparation methods, have had a tremendous impact on cell biology.

Electron tomography (ET) is a general approach to obtain three-dimensional (3D) information. It is based on an old concept, in which projection images of vitrified specimens are acquired with an electron microscope by tilting the specimen through a range of tilt angles (typically −60° to +60°) at a pre-defined interval (Hoppe et al., 1974; Baumeister et al., 1999). In cryo-ET, the stack of acquired projections can be further processed to yield a 3D volume (a tomogram) that represents the block of vitreous ice in which the specimen is embedded (Baumeister et al., 1999; Murphy and Jensen, 2007). This volume can then be analyzed by visual inspection and segmentation of specific elements of interest (for example, actin filaments, microtubules and macromolecules), or by extracting and averaging multiple instances of individual components to obtain a medium-to-high resolution structure (reviewed in Briggs, 2013).

Cryo-ET has matured into a reliable method for obtaining a structural blueprint of the unperturbed macromolecular organization inside cells at a resolution of a few nanometers (Woodward et al., 2015; Stauffer et al., 2014; Elad et al., 2013; Fridman et al., 2012; Patla et al., 2010; Carlson et al., 2010). Here, we focus on the study of macromolecules, organelles, entire cells and multi-cell specimens, primarily from the Eukaryotic kingdom, and discuss some of the recent advances and applications of this technique that make it possible to obtain a realistic view of cellular landscapes in their physiological environment.

Cryo-ET of macromolecules – pushing the resolution for structural determination

Single-particle cryo-EM has a long-standing reputation in achieving near-atomic resolution structures, provided that the specimen has optimal size, conformational homogeneity (reviewed in Cheng et al., 2015), symmetry (as is the case with many viruses) and can be detected under the electron beam. This method takes advantage of the high number of particles captured in varying orientations within two-dimensional (2D) projection images to create a final 3D density map.

Charge-coupled detectors (CCDs) have been instrumental for image acquisition. In CCDs, the electrons first pass through a scintillator, where they are converted into photons, that then travel through a fiber-optic bundle before being recognized by the sensor; however, this causes information degradation, which is manifested at the high frequency ranges. The recent introduction of direct detector device (DDD) cameras (Li et al., 2013; Faruqi and McMullan, 2011; Milazzo et al., 2011; Ruskin et al., 2013; Bammes et al., 2012) is revolutionizing the field of cryo-EM and cryo-ET. In comparison to CCDs, DDDs have a complementary metal-oxide semiconductor (CMOS) chip that is able to directly recognize electrons. Therefore, DDDs are able to better retrieve high-frequency information. DDDs also benefit from having a high frame rate, which allows for rapid acquisition of multiple projections of the same area within a short period of time. In turn, this allows for image processing, such as fine-tuning of the data by performing motion (or drift) correction. With the help of DDDs, single-particle cryo-EM can now routinely resolve molecular

[1]Department of Biochemistry, University of Zurich, Winterthurerstrasse 190, Zurich 8057, Switzerland. [2]Department of Life Sciences and the National Institute for Biotechnology in the Negev, Ben-Gurion University, Beer-Sheva 84105, Israel.

*Author for correspondence (omedalia@bioc.uzh.ch)

Journal of Cell Science (2016) 129, 469-476 doi:10.1242/jcs.171967

assemblies to 3–4 Å, with the highest reported resolution to date of 2.2 Å (Bartesaghi et al., 2015).

For cryo-ET, the resolution has been much lower (~20 Å), even when subtomogram averaging is applied. Subtomogram averaging involves the alignment and averaging of multiple instances of the macromolecule of interest (for example, ribosomes from a cell). First, the macromolecules are identified within the tomogram and then computationally extracted, such that each subvolume contains only one instance of the macromolecule. The computationally extracted subvolumes are also known as subtomograms. Subtomogram averaging, just as is the case in single-particle cryo-EM, relies on the structural homogeneity of specimens. Subtomograms are aligned in an iterative fashion either to an external initial model or to an initial model generated from the data itself. After the alignment is completed, the subtomograms are averaged together to generate a final 3D density map. An example of subtomogram averaging to subnanometer resolution is the recent work by Schur et al.; here, cryo-ET and optimized subtomogram averaging methods were applied to determine the structure of the capsid lattice within purified, intact immature human immunodeficiency virus type 1 (HIV-1) virions (Fig. 1A; Schur et al., 2015). At 8.8 Å, the structure of the capsid proteins is sufficiently resolved to allow for the unambiguous positioning of all α-helices (Fig. 1B–D), which provided a glimpse into the tertiary and quaternary structural interactions that are involved in the assembly of the virus.

Subtomogram averaging can also be applied to molecular machines that exhibit several conformational states, namely discrete heterogeneity. Individual subtomograms can be sorted into different classes based on how similar or different they look compared to one or more models (Shahmoradian et al., 2013; Darrow et al., 2015). However, because of the highly dynamic nature of most cellular components, it remains challenging to achieve subnanometer resolution by cryo-ET. Nevertheless, even at lower resolution, valuable structural and functional information can be deduced, which often cannot be accomplished with biochemistry alone or by other structural methods. Such information can give important insight into crucial cellular processes. For example, for years, the integrity of the 26S proteasome as a double-headed structure was questioned. The 26S proteasome is a key player in eukaryotic protein quality control and in the regulation of numerous cellular processes; however, it is also a highly dynamic molecular machine. Using quantitative *in situ* structural studies of intact hippocampal neurons, the ratio between single- and double-capped proteasomes and the conformational states of individual complexes could be determined. Hence, Asano et al. were able to show that, in the absence of proteotoxic stress, only 20% of the 26S proteasomes were engaged in substrate processing, whereas the rest were in the substrate-accepting ground state (Asano et al., 2015). These cryo-ET findings suggest that, in the absence of stress, the proteasome system is not utilized to its full capacity and that the single-capped 26S proteasome is indeed physiologically relevant, rather than constituting a biochemical purification artifact.

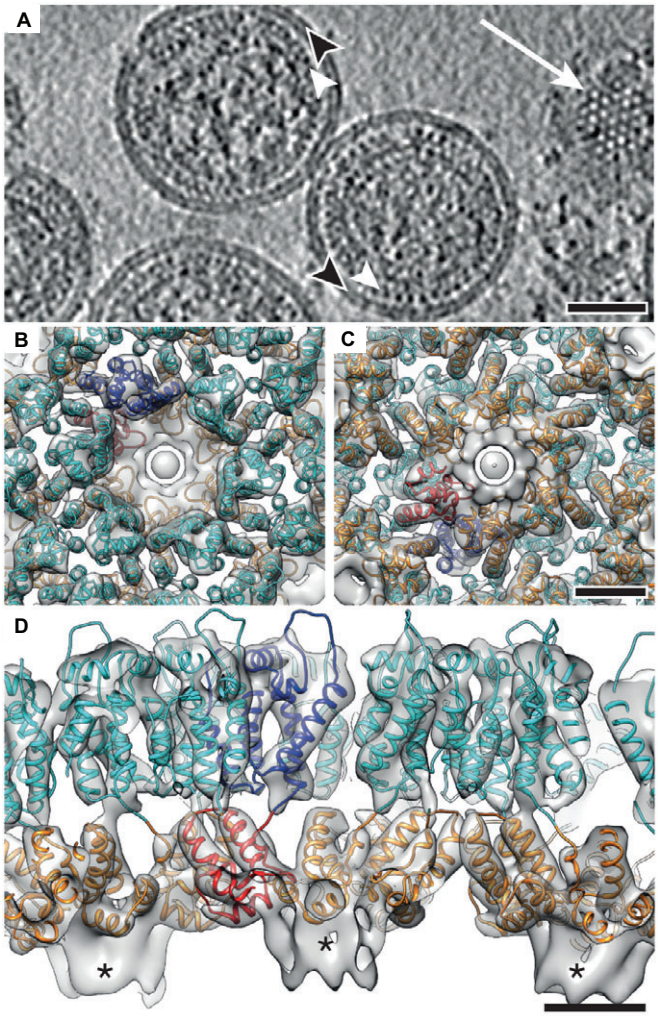

Fig. 1. The structure of the capsid lattice of immature HIV-1 virions. (A) A tomographic slice of immature HIV-1 particles treated with amprenavir. The immature capsid layer is denoted by white and the viral membrane by black arrowheads. The white arrow shows the hexagonal capsid lattice. Scale bar: 50 nm. The structure of the immature capsid lattice viewed from outside (B) and from inside the virus (C). (D) Orthogonal view of the capsid lattice. High-resolution structures for the N- (cyan) and C-terminal domains (orange) have been fitted into the density. Red and blue represent an individual capsid monomer. Unfilled densities marked with asterisks correspond to the regions occupied by one of the spacer peptides, which is positioned between the capsid and nucleocapsid domain in the Gag polyprotein. Scale bar: 25 Å. Modified with permission from Schur et al., 2015.

Cryo-ET of macromolecular assemblies within organelles – the nuclear pore complex

A unique and important task of cryo-ET is to structurally analyze macromolecular assemblies within organelles and cells, especially those that are challenging to purify. One such example is the structural analysis of the nuclear envelope. Here, cryo-ET has been instrumental for studying the structure of the nuclear pore complex (NPC) (Grossman et al., 2012) and the underlying nuclear lamina (Gruenbaum and Medalia, 2015). The nuclear membrane consists of two lipid bilayers, which are perforated by NPCs that serve as selective gates between the nucleus and cytoplasm of a cell. This enables the selective diffusion of the most essential molecules into the nucleus and, at the same time, transport of RNA and ribosomal proteins to the cytoplasm. The NPC is composed of multiple copies of about 30 different proteins (nucleoporins). The extremely large size (~120 MDa in vertebrates), coupled with the difficulty to purify NPCs biochemically, make the NPC a particularly challenging specimen for structural studies. However, to fully appreciate the transport mechanism facilitated by this molecular machine, a detailed structural analysis is necessary. The study of the NPC by cryo-ET has been of great interest over the last decade (Stoffler et al., 2003; Beck et al., 2004, 2007; Maimon et al., 2012; von Appen et al., 2015); however, advancements in imaging and

Journal of Cell Science (2016) 129, 469-476 doi:10.1242/jcs.171967

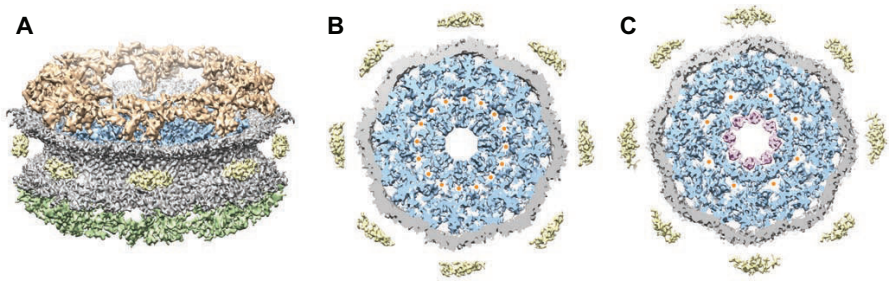

Fig. 2. Structural analysis of the *X. laevis* NPC. (A) Surface-rendered view of the NPC. The central channel of the native (B) compared with the ActD-treated NPC averaged structure (C) as determined by cryo-ET. The spoke ring and the central channel ring are depicted in blue, the nuclear envelope in gray and the luminal densities in yellow. The inner pore ring of the ActD-treated NPC adopts a distinct structure, shown in purple. Channels marked with orange dots are ~2 nm in diameter. Modified with permission from Eibauer et al., 2015.

data processing in the past few years have helped to make a significant leap in resolution and, therefore, our understanding of the mechanics of the NPC. For instance, our recent study of NPCs in *Xenopus laevis* oocytes has revealed the structure of two distinct NPC states (Fig. 2): the native NPC, without any chemical treatment or fixation (Fig. 2A,B), and a reduced-transport state in Actinomycin D (ActD)-treated NPCs (Fig. 2C) (Eibauer et al., 2015). As ActD treatment inhibits RNA transcription, and therefore RNA transport, ActD NPCs represent NPCs that are in a relaxed state. Both the native and ActD NPCs from *X. laevis* oocytes were resolved by cryo-ET and subtomogram averaging to ~20 Å. Although the central channel is mainly composed of flexible components, we were able to visualize these assemblies and detected structural changes within the inner ring, when transcription was halted (Fig. 2B,C). This study provided new insights into the architecture of the central channel of the NPC and the possible transport routes through the pore. With the current state of technology, it is therefore feasible that, in the next few years, a pseudo-atomic map of this complex could be resolved, which will help to elucidate the complex process of cytoplasmic–nuclear transport.

Cellular tomography

Revealing the molecular organization of cells in a physiologically relevant state is crucial in order to acquire a deeper understanding of cell biology. Cellular processes, such as cell adhesion and mitosis, can be investigated by cryo-ET. This approach can also be used to observe the cytoskeleton (Kürner et al., 2004; Medalia et al., 2002, 2007) and its morphology during interactions with viruses and parasites (Grünewald and Cyrklaff, 2006; Small, 2015; Hanssen et al., 2013; Ben-Harush et al., 2010).

Early studies of the actin cytoskeleton were mostly focused on morphological observations within the EM data (reviewed in Medalia and Geiger, 2010). By imaging intact, vitrified cells, the cytoskeletal organization can be observed in a near-native environment, undisturbed by preparation procedures that are required for conventional EM, such as detergent extraction, chemical fixation, dehydration, metal coating and critical point drying (Svitkina, 2010; Horne and Wildy, 1979; Glauert and Lewis, 1998). Actin filaments have been extensively studied *in vitro* (Galkin et al., 2015); however, less information is available about the precise organization of the actin network *in vivo*. With the recent advances in cryo-ET, we can now evaluate some filament properties within cells and even detect the helical pitch of individual actin filaments (Fig. 3A,B). This makes it possible to determine the polarity of each actin filament within the cytoskeletal network. Such information would help to decipher the mechanical properties of cytoskeleton-based processes, such as focal adhesion and stress fiber formation (Patla et al., 2010; Geiger et al., 2009), interactions with other cells and cell migration. For example, high-resolution data can help identify the polymerization sites of actin in maturing focal adhesions, which in turn could elucidate their local function (Narita et al., 2012). Other dynamic cytoskeletal components, such as microtubules, can also be observed by cryo-ET (Fig. 3C, compare to Koning, 2010).

An elegant application of cellular cryo-ET is the study of the trypanosome flagellum – a complex, microtubule-based nanomachine (Koyfman et al., 2011). *Trypanosoma brucei* is a

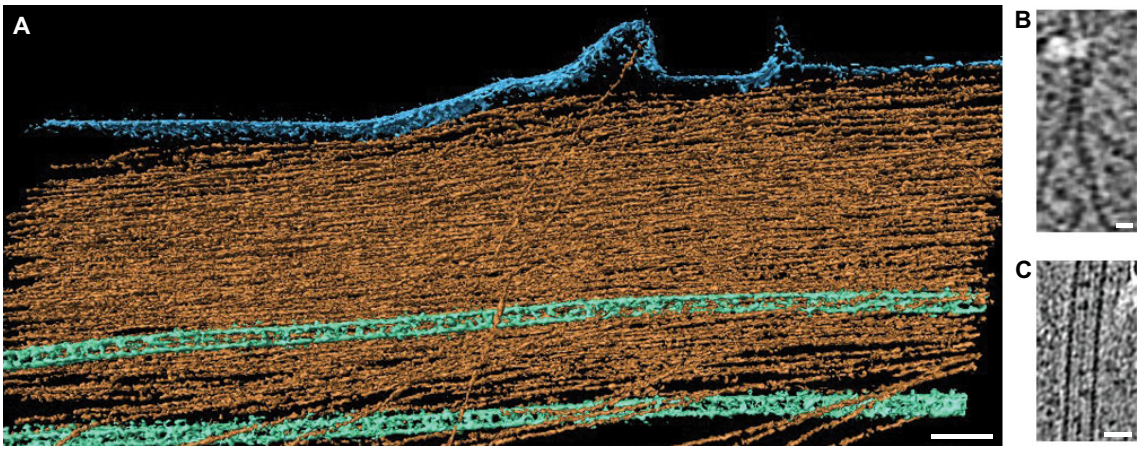

Fig. 3. Analyzing the cytoskeleton inside intact rat embryotic fibroblasts and close-up view of individual cytoskeletal filaments. (A) Surface-rendered view of a reconstructed area underneath the plasma membrane. Plasma membrane (blue) and microtubules (turquoise) were rendered manually. Actin filaments (orange) were rendered using an automated actin segmentation package. Scale bar: 100 nm. (B) Close-up of a region of a tomogram similar to the one in A, with two actin filaments showing the actin substructure, namely the helical appearance that results from the arrangement of multiple actin monomers. Scale bar: 20 nm. (C) Close-up of a representative microtubule from a different tomogram. Scale bar: 24 nm.

Journal of Cell Science (2016) 129, 469-476 doi:10.1242/jcs.171967

parasite that causes African sleeping sickness. Its flagellum is essential for the lifecycle and infection ability of the parasite, and it is being explored as a potential drug target. The flagellum contains a microtubular azoneme, a crystalline paraflagellar rod and connecting proteins (PFR). Subtomogram averaging revealed the typical nine microtubule doublets arranged around a central microtubule pair, as well as the structure of the flagellum in three different bending states (Koyfman et al., 2011). Here, analysis of the bent flagella made it possible to suggest a model for the locomotion pattern of the parasite, in which the PFR functions like a jackscrew and modifies the in-plane axoneme motion, resulting in the characteristic bihelical motility of the trypanosome.

Improved EM optics impact on what we see inside the cell

EM is mainly limited by how far electrons can penetrate through the biological sample, restricting the thickness of the specimen to be examined to less than 1 µm. This generally limits the type of specimens that can be imaged by EM to isolated viruses (Hong et al., 2015; Murata et al., 2010; Dai et al., 2010), protein complexes (Koyfman et al., 2011; Nickell et al., 2007a,b), organelles (Eibauer et al., 2015; Nicastro et al., 2000; Beck et al., 2007, 2004), smaller prokaryotic cells (Briegel et al., 2015; Zhao et al., 2014) and thin peripheral regions of eukaryotic cells (Hu, 2014; Ben-Harush et al., 2010; Patla et al., 2010; Cyrklaff et al., 2007). Cells up to 1 µm in thickness can be imaged by EM, as shown for *Ostreococcus tauri*, the smallest eukaryotic cell (Henderson et al., 2007); this has provided a unique insight into the ultrastructure and characteristics of the cells during different stages of their cell cycle. The newly available phase plate technology for EM provides increased image contrast and therefore, makes it easier to identify fine cellular components within thicker specimens *in situ* (Dai et al., 2013, 2014). Phase plates are typically positioned in the back focal plane of the objective lens of the EM and shift the phase of the scattered electron beam such that low-frequency information is amplified. This is the information that contributes to image contrast, and higher contrast makes it possible to detect structural features within the data and, therefore, allows for the direct observation and analysis of the internal 3D structure of cells (Asano et al., 2015; Fukuda et al., 2015; Engel et al., 2015a,b; Dai et al., 2014, 2013) (Fig. 4).

Structural analysis of multicellular systems

In order to examine bulkier specimens, the sample has to be either mechanically trimmed or thinned by a focused ion beam. Cryo-sectioning of frozen hydrated specimens (CEMOVIS) is one approach to obtain sections that are sufficiently thin for EM. In this method, frozen hydrated cells or tissues of interest are sectioned with a diamond knife resulting in samples with a thickness of 40–100 µm (Al-Amoudi et al., 2004). Samples that have been studied by CEMOVIS thus far include mitochondria (Hsieh et al., 2006), human skin (Al-Amoudi et al., 2007; Al-Amoudi and Frangakis, 2008), microtubules (Bouchet-Marquis et al., 2007), bacteria (Delgado et al., 2013; Zuber et al., 2008) and bacterial spores (Couture-Tosi et al., 2010; Dittmann et al., 2015). However, this technique has its limitations, mainly due to compression of the thin sections in the direction of cutting, which can complicate the proper interpretation of the data (Al-Amoudi et al., 2005).

More recently, cryo-focused ion beam scanning electron microscopy (cryo-FIB-SEM) has emerged as an alternative to conventional sample-thinning methods. It incorporates specimen vitrification and yields thin lamellae (200–500 nm) from cells grown on EM grids, which can then be imaged by cryo-ET (Marko et al., 2007; Rigort et al., 2012). Cryo-ET of a FIB-milled *Dictyostelium discoideum* cell revealed the nuclear envelope with the NPCs, the endoplasmic reticulum, mitochondria, microtubules, vacuolar compartment and ribosomes all embedded within the lamella region

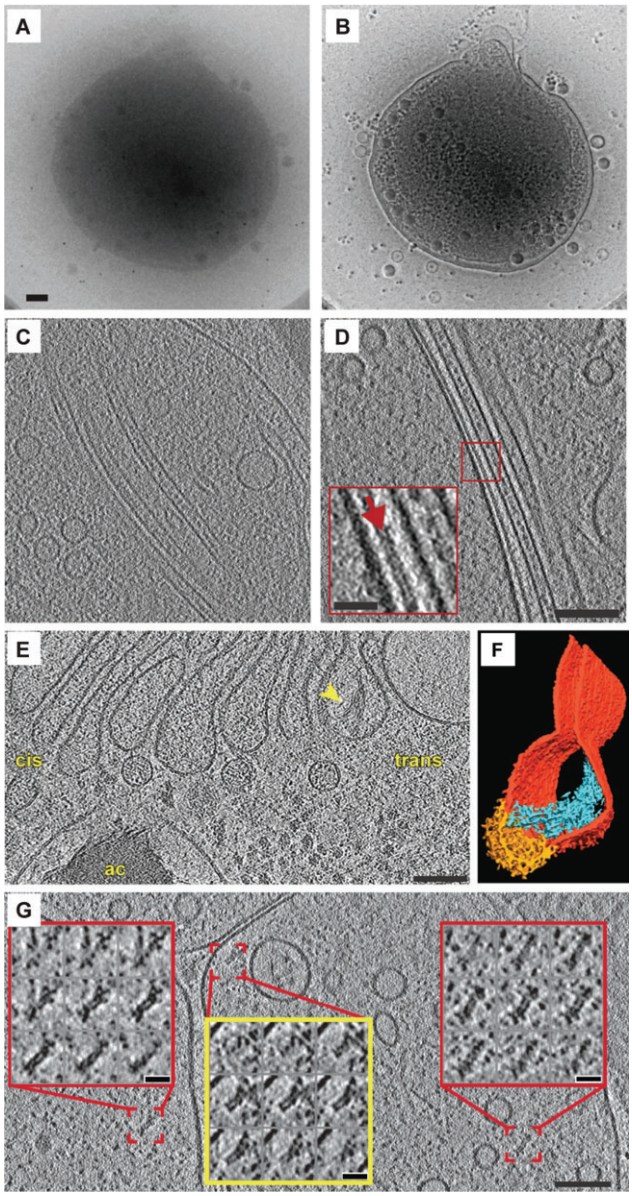

Fig. 4. Examples of cellular tomography performed with phase plates. (A,B) Cryo-ET projections of a Syn5-infected cyanobacterium cell without (A) and with (B) a phase plate under identical imaging conditions. Scale bar: 100 nm. Modified with permission from Dai et al., 2013. (C,D) Projections of a tomogram of primary cultured neurons without (C) and with phase plate (D). The red arrow in D indicates the lipid bilayer. Scale bar: 100 nm (20 nm inset). Modified with permission from Fukuda et al., 2015. (E) A slice of a tomogram acquired with a phase plate showing an intracisternal filament bundle within the cisternae of the trans-Golgi (yellow arrow) and a nearby coated bud. An acidocalcisome containing a dense aggregate of polyphosphate filaments is labeled with 'ac'. Scale bar is 100 nm. (F) Segmentation of the cisterna in E, with the Golgi membrane in dark orange, the coated bud in yellow and the filament bundle in blue. Panels E and F were modified with permission from Engel et al., 2015a. (G) A slice from a tomogram of a cultured hippocampal neuronal cell. The colored squares are zoomed-in views and show magnified slices through individual proteasome volumes of a single-capped (yellow box, middle) and two double-capped (red boxes, left and right) 26S proteasomes. Scale bars: 100 nm (25 nm inset). Modified with permission from Asano et al., 2015.

Journal of Cell Science (2016) 129, 469-476 doi:10.1242/jcs.171967

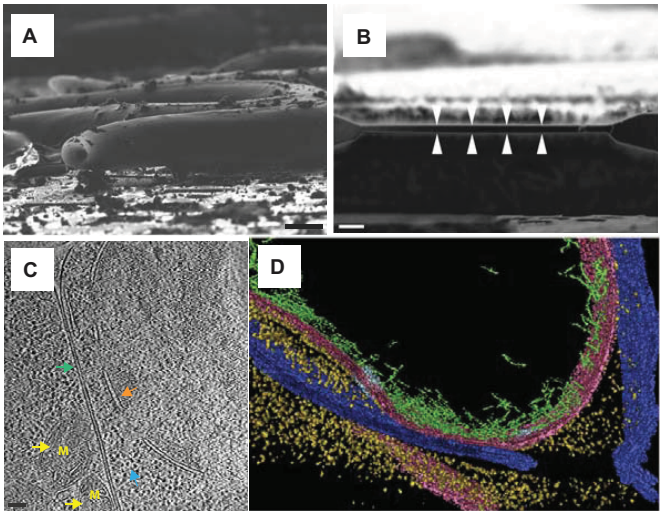

Fig. 5. Cryo-FIB milling and cryo-ET of *C. elegans*. (A) Scanning EM (SEM) image of an adult *C. elegans* worm that has been vitrified by high-pressure freezing, using 2-methylpentane as freezing medium. Scale bar: 10 µm. (B) A lamella of the adult worm (arrowheads) shown in A, produced by cryo-FIB milling. Scale bar: 2 µm. (C) A slice through a tomogram of a FIB-milled *C. elegans* embryo; here, the plasma membrane (green arrow), mitochondria (yellow arrows; 'M'), ribosomes (blue arrow) and the nuclear envelope (orange arrow) can be seen. Scale bar: 100 nm. (D) An example of a rendering of another tomogram acquired on a *C. elegans* embryo lamella. Shown here are the plasma membrane (dark blue), nuclear envelope (pink), ribosomes (gold), NPCs (blue) and filamentous structures near the inner nuclear membrane (green). Modified with permission from Harapin et al., 2015.

of interest (Rigort et al., 2012). This technique has also recently been used to acquire 3D structural information for the distribution of ER–mitochondrial contacts in mammalian cells and provide insights into the localization of mitochondrial constriction sites and the existence of two types of membrane associations between the two organelles (Ohta et al., 2014). This procedure can also be applied to tissues such as skeletal muscle (Wagenknecht et al., 2015), thereby enabling the visualization of natively preserved regions of interest that cannot be purified. The first 3D-snapshots of the algal chloroplast were also obtained by this method, affording a glimpse into photosynthesis, thylakoid biogenesis and carbon fixation (Engel et al., 2015b).

FIB milling and imaging by cryo-ET of frozen *Caenorhabditis elegans* embryos and adult worms has allowed researchers to visualize the intracellular organization during particular stages of development in tissues of interest (Harapin et al., 2015). Here, the milled lamellae were ∼330 nm thick in the case of embryos, and ∼660 nm thick for adult worms, both sufficiently thin to be visualized by cryo-ET (Fig. 5). Furthermore, *C. elegans* embryos were fluorescently labeled during the preparation, which allowed the identification of proteins on the surface of thin cryo-lamellae by correlative light and electron microscopy (CLEM). Combining CLEM with cryo-FIB-SEM (Mahamid et al., 2015) and cryo-ET can also be applied to explore the structure of macromolecular complexes *in situ* during various stages of development, which will present further details about processes occurring in more complex organisms. Furthermore, the use of FIB-SEM to generate thin enough samples for cryo-ET has the potential to eventually bridge the gap between developmental and structural biology, by resolving with high reliability embryonic structures at different developmental stages.

Cryo-FIB can also be combined with phase plate cryo-ET (Fukuda et al., 2015), as performed in a recent study of *Chlamydomonas* cells (Engel et al., 2015a). Here, the authors obtained a remarkable view of the Golgi ultrastructure that revealed new components of the Golgi cisternae within unperturbed cells with an unprecedented resolution (Engel et al., 2015a) (Fig. 4E). Although not yet routinely used, we anticipate that in the near future, combining cryo-FIB and phase plates might have a tremendous impact on structural studies of multi-cellular specimens.

Combining correlative light and electron microscopy

One limitation of cryo-ET is the inability to unambiguously identify the position of a protein or a process within the cell because of the low signal-to-noise ratio of cryo-embedded specimens. Moreover, cryo-tomograms have a limited field of view of 1 to 2 µm^2, which only covers a very small fraction of a typical eukaryotic cell. Using CLEM, it has been possible to capitalize on the advantages of both underlying techniques (Schorb and Briggs, 2014) and tackle biological questions that cannot be resolved by either approach alone; specific molecules and thus particular events are localized with fluorescence-based microscopy, then cryo-tomograms are acquired to reveal the cellular ultrastructure at these sites.

Cryo-CLEM has the benefit of preserving specimens (e.g. whole cells or bacteria) in a near-native state, while still using fluorescent labels to identify specific regions of interest. Recently, this method was successfully applied to vitrified *Streptomyces* bacteria to study cell division (Koning et al., 2014).

Cryo-ET as a medical diagnostics tool

Cryo-ET could be also used as a diagnostics tool and help resolve molecular differences between healthy and diseased states. The first reported instance of using human clinical samples for cryo-ET studies was the structural analysis of human cilia that were isolated from airway epithelial cells from both healthy individuals and patients with primary ciliary dyskinesia (PCD) (Lin et al., 2014). Diagnosing PCD has traditionally relied on analysis by conventional EM and detection of defects in mobile cilia. However, a third of PCD patients have cilia that appear normal under the EM, perhaps due to the harsh preparation methods required for conventional imaging. This new study built on the existing knowledge about human cilia and helped elucidate structural defects associated with PCD and other ciliopathies. Applying cryo-ET and subtomogram averaging to human ciliary axonemes from healthy individuals resulted in an improved resolution over conventional EM studies that utilized chemically fixed samples. The averaged cryo-ET structure showed that the overall architecture is similar to that of the motile cilia and flagella of other organisms (Lin et al., 2014). However, subtomogram averaging of samples derived from patients with mutated cilia pointed to small structural differences compared to healthy cilia, which could explain why the particular variant studied resulted in a clinically attenuated phenotype, where patients experience delayed onset of pulmonary symptoms and maintain better lung function compared to patients with mutations in other genes.

Platelet biology is another field that is benefiting from structural studies using EM (reviewed in Sorrentino et al., 2015). Recently, Wang et al. have illustrated how cryo-ET can be utilized as a non-invasive method to detect structural biomarkers of diseases that affect platelets (Wang et al., 2015). For example, it is known that the count and functionality of platelets can be altered in cancer patients. The team evaluated frozen-hydrated platelets from patients with newly diagnosed invasive ovarian cancer and from control subjects (patients with benign masses and healthy individuals) and analyzed the morphologic features of each sample. The visual differences were quantified by measuring length, area and/or the number of observed

cellular features, such as microtubule length, number of mitochondria and granules, platelet area, etc. Interestingly, the number of mitochondria in diseased patients was about 50% higher and the length of their microtubules was significantly shorter compared to the control group. Based on their analysis, the team designed a predictive model, where malignancy was predicted solely by analyzing the number of mitochondria and the microtubule length in platelets. Malignancy was correctly assigned in 20 of 23 cases (87%), indicating that the ultrastructure of platelets could be a valuable tool, in the future, for detecting ovarian cancer (Wang et al., 2015).

The future of cryo-ET

Cryo-ET is establishing itself as an invaluable technique for structural cellular biology. A big milestone for cryo-ET will be to routinely reach subnanometer resolution. Such a resolution will be sufficient to unambiguously fit existing X-ray crystallography and NMR data into the EM densities of larger macromolecular assemblies, which will help build more realistic atomistic models of these macromolecules and provide a glimpse into their inter-organization and function.

Proof-of-concept studies on the GroEL chaperonin yielded the first subnanometer resolution structure that utilized cryo-ET (Bartesaghi et al., 2012). Subsequently, Schur et al. resolved the highly symmetric immature HIV-1 capsid in intact virus particles by subtomograms averaging to 8.8 Å resolution and outlined an approach that might be helpful in determining the structures of other macromolecules within heterogeneous environments to subnanometer resolution (Schur et al., 2015).

The continuous advancement of both imaging and image processing also has a big impact on the data and the quality of the reconstructions we can obtain today compared to only a few years ago (reviewed in Bai et al., 2015). The new direct electron detectors provide higher resolution data. Advanced image processing helps to compensate for aberrations and artifacts that are associated with the data, which in turn yields structures that are of higher quality.

Owing to these advancements, we are on the brink of a myriad of new information that will revolutionize *in vivo* structure analysis and the way we think about structural cellular biology. The future of cryo-ET lies in the routine observation of cellular features of interest within their native environment, in combination with (when applicable) other upcoming structural techniques such as CLEM and FIB, and in utilizing state-of-the-art data processing to obtain structures of these features at subnanometer resolution. This is an exciting time for cell biology and will most certainly have an impact on how we 'see' cells and thus refine our view of the molecular assemblies that drive cellular processes.

Acknowledgements

We thank Sarah Stauffer and Tanuj Sapra for their critical reading of the manuscript.

Competing interests

The authors declare no competing or financial interests.

Funding

This work was supported by a European Research Council (ERC) Starting Grant [grant number 243047 INCEL]; a Swiss National Science Foundation Grant [grant number SNSF 31003A 159706/1]; and the Mäxi Foundation.

References

Al-Amoudi, A. and Frangakis, A. S. (2008). Structural studies on desmosomes. *Biochem. Soc. Trans.* **36**, 181-187.

Al-Amoudi, A., Norlen, L. P. O. and Dubochet, J. (2004). Cryo-electron microscopy of vitreous sections of native biological cells and tissues. *J. Struct. Biol.* **148**, 131-135.

Al-Amoudi, A., Studer, D. and Dubochet, J. (2005). Cutting artefacts and cutting process in vitreous sections for cryo-electron microscopy. *J. Struct. Biol.* **150**, 109-121.

Al-Amoudi, A., Díez, D. C., Betts, M. J. and Frangakis, A. S. (2007). The molecular architecture of cadherins in native epidermal desmosomes. *Nature* **450**, 832-837.

Asano, S., Fukuda, Y., Beck, F., Aufderheide, A., Förster, F., Danev, R. and Baumeister, W. (2015). Proteasomes. A molecular census of 26S proteasomes in intact neurons. *Science* **347**, 439-442.

Bai, X.-C., McMullan, G. and Scheres, S. H. W. (2015). How cryo-EM is revolutionizing structural biology. *Trends Biochem. Sci.* **40**, 49-57.

Bammes, B. E., Rochat, R. H., Jakana, J., Chen, D.-H. and Chiu, W. (2012). Direct electron detection yields cryo-EM reconstructions at resolutions beyond 3/4 Nyquist frequency. *J. Struct. Biol.* **177**, 589-601.

Bartesaghi, A., Lecumberry, F., Sapiro, G. and Subramaniam, S. (2012). Protein secondary structure determination by constrained single-particle cryo-electron tomography. *Structure* **20**, 2003-2013.

Bartesaghi, A., Merk, A., Banerjee, S., Matthies, D., Wu, X., Milne, J. L. and Subramaniam, S. (2015). 2.2 Å resolution cryo-EM structure of β-galactosidase in complex with a cell-permeant inhibitor. *Science* **348**, 1147-1151.

Baumeister, W., Grimm, R. and Walz, J. (1999). Electron tomography of molecules and cells. *Trends Cell Biol.* **9**, 81-85.

Beck, M., Förster, F., Ecke, M., Plitzko, J. M., Melchior, F., Gerisch, G., Baumeister, W. and Medalia, O. (2004). Nuclear pore complex structure and dynamics revealed by cryoelectron tomography. *Science* **306**, 1387-1390.

Beck, M., Lučić, V., Förster, F., Baumeister, W. and Medalia, O. (2007). Snapshots of nuclear pore complexes in action captured by cryo-electron tomography. *Nature* **449**, 611-615.

Ben-Harush, K., Maimon, T., Patla, I., Villa, E. and Medalia, O. (2010). Visualizing cellular processes at the molecular level by cryo-electron tomography. *J. Cell Sci.* **123**, 7-12.

Bouchet-Marquis, C., Zuber, B., Glynn, A.-M., Eltsov, M., Grabenbauer, M., Goldie, K. N., Thomas, D., Frangakis, A. S., Dubochet, J. and Chrétien, D. (2007). Visualization of cell microtubules in their native state. *Biol. Cell* **99**, 45-53.

Briegel, A., Ortega, D. R., Huang, A. N., Oikonomou, C. M., Gunsalus, R. P. and Jensen, G. J. (2015). Structural conservation of chemotaxis machinery across Archaea and Bacteria. *Environ. Microbiol. Rep.* **7**, 414-419.

Briggs, J. A. G. (2013). Structural biology in situ—the potential of subtomogram averaging. *Curr. Opin. Struct. Biol.* **23**, 261-267.

Carlson, L.-A., de Marco, A., Oberwinkler, H., Habermann, A., Briggs, J. A. G., Kräusslich, H.-G. and Grünewald, K. (2010). Cryo electron tomography of native HIV-1 budding sites. *PLoS Pathog.* **6**, e1001173.

Cheng, Y., Grigorieff, N., Penczek, P. A. and Walz, T. (2015). A primer to single-particle cryo-electron microscopy. *Cell* **161**, 438-449.

Couture-Tosi, E., Ranck, J.-L., Haustant, G., Pehau-Arnaudet, G. and Sachse, M. (2010). CEMOVIS on a pathogen: analysis of Bacillus anthracis spores. *Biol. Cell* **102**, 609-619.

Cyrklaff, M., Linaroudis, A., Boicu, M., Chlanda, P., Baumeister, W., Griffiths, G. and Krijnse-Locker, J. (2007). Whole cell cryo-electron tomography reveals distinct disassembly intermediates of vaccinia virus. *PLoS ONE* **2**, e420.

Dai, W., Hodes, A., Hui, W. H., Gingery, M., Miller, J. F. and Zhou, Z. H. (2010). Three-dimensional structure of tropism-switching Bordetella bacteriophage. *Proc. Natl. Acad. Sci. USA* **107**, 4347-4352.

Dai, W., Fu, C., Raytcheva, D., Flanagan, J., Khant, H. A., Liu, X., Rochat, R. H., Haase-Pettingell, C., Piret, J., Ludtke, S. J. et al. (2013). Visualizing virus assembly intermediates inside marine cyanobacteria. *Nature* **502**, 707-710.

Dai, W., Schmid, M. F., King, J. A. and Chiu, W. (2014). Identifying the assembly pathway of cyanophage inside the marine bacterium using electron cryo-tomography. *Microb. Cell* **1**, 45-47.

Darrow, M. C., Sergeeva, O. A., Isas, J. M., Galaz-Montoya, J. G., King, J. A., Langen, R., Schmid, M. F. and Chiu, W. (2015). Structural mechanisms of mutant huntingtin aggregation suppression by the synthetic chaperonin-like CCT5 complex explained by cryoelectron tomography. *J. Biol. Chem.* **290**, 17451-17461.

Delgado, L., Carrión, O., Martínez, G., López-Iglesias, C. and Mercadé, E. (2013). The stack: a new bacterial structure analyzed in the Antarctic bacterium Pseudomonas deceptionensis M1T by transmission electron microscopy and tomography. *PLoS ONE* **8**, e73297.

Dittmann, C., Han, H.-M., Grabenbauer, M. and Laue, M. (2015). Dormant Bacillus spores protect their DNA in crystalline nucleoids against environmental stress. *J. Struct. Biol.* **191**, 156-164.

Eibauer, M., Pellanda, M., Turgay, Y., Dubrovsky, A., Wild, A. and Medalia, O. (2015). Structure and gating of the nuclear pore complex. *Nat. Commun.* **6**, 7532.

Elad, N., Volberg, T., Patla, I., Hirschfeld-Warneken, V., Grashoff, C., Spatz, J. P., Fässler, R., Geiger, B. and Medalia, O. (2013). The role of integrin-linked kinase in the molecular architecture of focal adhesions. *J. Cell Sci.* **126**, 4099-4107.

Engel, B. D., Schaffer, M., Albert, S., Asano, S., Plitzko, J. M. and Baumeister, W. (2015a). In situ structural analysis of Golgi intracisternal protein arrays. *Proc. Natl. Acad. Sci. USA* **112**, 11264-11269.

Engel, B. D., Schaffer, M., Kuhn Cuellar, L., Villa, E., Plitzko, J. M. and Baumeister, W. (2015b). Native architecture of the Chlamydomonas chloroplast revealed by in situ cryo-electron tomography. *eLife* **4**, e04889.
Faruqi, A. R. and McMullan, G. (2011). Electronic detectors for electron microscopy. *Q. Rev. Biophys.* **44**, 357-390.
Fridman, K., Mader, A., Zwerger, M., Elia, N. and Medalia, O. (2012). Advances in tomography: probing the molecular architecture of cells. *Nat. Rev. Mol. Cell Biol.* **13**, 736-742.
Fukuda, Y., Laugks, U., Lučić, V., Baumeister, W. and Danev, R. (2015). Electron cryotomography of vitrified cells with a Volta phase plate. *J. Struct. Biol.* **190**, 143-154.
Galkin, V. E., Orlova, A., Vos, M. R., Schröder, G. F. and Egelman, E. H. (2015). Near-atomic resolution for one state of F-actin. *Structure* **23**, 173-182.
Geiger, B., Spatz, J. P. and Bershadsky, A. D. (2009). Environmental sensing through focal adhesions. *Nat. Rev. Mol. Cell Biol.* **10**, 21-33.
Glauert, A. M. and Lewis, P. R. (1998). *Biological Specimen Preparation for Transmission Electron Microscopy. Practical Methods in Electron Microscopy*, Vol. 17. Princeton University Press.
Grossman, E., Medalia, O. and Zwerger, M. (2012). Functional architecture of the nuclear pore complex. *Annu. Rev. Biophys.* **41**, 557-584.
Gruenbaum, Y. and Medalia, O. (2015). Lamins: the structure and protein complexes. *Curr. Opin. Cell Biol.* **32**, 7-12.
Grünewald, K. and Cyrklaff, M. (2006). Structure of complex viruses and virus-infected cells by electron cryo tomography. *Curr. Opin. Microbiol.* **9**, 437-442.
Hanssen, E., Dekiwadia, C., Riglar, D. T., Rug, M., Lemgruber, L., Cowman, A. F., Cyrklaff, M., Kudryashev, M., Frischknecht, F., Baum, J. et al. (2013). Electron tomography of Plasmodium falciparum merozoites reveals core cellular events that underpin erythrocyte invasion. *Cell. Microbiol.* **15**, 1457-1472.
Harapin, J., Börmel, M., Sapra, K. T., Brunner, D., Kaech, A. and Medalia, O. (2015). Structural analysis of multicellular organisms with cryo-electron tomography. *Nat. Methods* **12**, 634-636.
Henderson, G. P., Gan, L. and Jensen, G. J. (2007). 3-D ultrastructure of O. tauri: electron cryotomography of an entire eukaryotic cell. *PLoS ONE* **2**, e749.
Hong, C., Pietilä, M. K., Fu, C. J., Schmid, M. F., Bamford, D. H. and Chiu, W. (2015). Lemon-shaped halo archaeal virus His1 with uniform tail but variable capsid structure. *Proc. Natl. Acad. Sci. USA* **112**, 2449-2454.
Hoppe, W., Gassmann, J., Hunsmann, N., Schramm, H. J. and Sturm, M. (1974). Three-dimensional reconstruction of individual negatively stained yeast fatty-acid synthetase molecules from tilt series in the electron microscope. *Hoppe-Seylers Z. Physiol. Chem.* **355**, 1483-1487.
Horne, R. W. and Wildy, P. (1979). An historical account of the development and applications of the negative staining technique to the electron microscopy of viruses. *J. Microsc.* **117**, 103-122.
Hsieh, C.-E., Leith, A., Mannella, C. A., Frank, J. and Marko, M. (2006). Towards high-resolution three-dimensional imaging of native mammalian tissue: electron tomography of frozen-hydrated rat liver sections. *J. Struct. Biol.* **153**, 1-13.
Hu, G.-B. (2014). Whole cell cryo-electron tomography suggests mitochondria divide by budding. *Microsc. Microanal.* **20**, 1180-1187.
Koning, R. I. (2010). Cryo-electron tomography of cellular microtubules. *Methods Cell Biol.* **97**, 455-473. Academic Press 2010.
Koning, R. I., Celler, K., Willemse, J., Bos, E., van Wezel, G. P. and Koster, A. J. (2014). Correlative cryo-fluorescence light microscopy and cryo-electron tomography of Streptomyces. *Methods Cell Biol.* **124**, 217-239.
Koyfman, A. Y., Schmid, M. F., Gheiratmand, L., Fu, C. J., Khant, H. A., Huang, D., He, C. Y. and Chiu, W. (2011). Structure of Trypanosoma brucei flagellum accounts for its bihelical motion. *Proc. Natl. Acad. Sci. USA* **108**, 11105-11108.
Kürner, J., Medalia, O., Linaroudis, A. A. and Baumeister, W. (2004). New insights into the structural organization of eukaryotic and prokaryotic cytoskeletons using cryo-electron tomography. *Exp. Cell Res.* **301**, 38-42.
Li, X., Mooney, P., Zheng, S., Booth, C. R., Braunfeld, M. B., Gubbens, S., Agard, D. A. and Cheng, Y. (2013). Electron counting and beam-induced motion correction enable near-atomic-resolution single-particle cryo-EM. *Nat. Methods* **10**, 584-590.
Lin, J., Yin, W., Smith, M. C., Song, K., Leigh, M. W., Zariwala, M. A., Knowles, M. R., Ostrowski, L. E. and Nicastro, D. (2014). Cryo-electron tomography reveals ciliary defects underlying human RSPH1 primary ciliary dyskinesia. *Nat. Commun.* **5**, 5727.
Mahamid, J., Schampers, R., Persoon, H., Hyman, A. A., Baumeister, W. and Plitzko, J. M. (2015). A focused ion beam milling and lift-out approach for site-specific preparation of frozen-hydrated lamellas from multicellular organisms. *J. Struct. Biol.* **192**, 262-269.
Maimon, T., Elad, N., Dahan, I. and Medalia, O. (2012). The human nuclear pore complex as revealed by cryo-electron tomography. *Structure* **20**, 998-1006.
Marko, M., Hsieh, C., Schalek, R., Frank, J. and Mannella, C. (2007). Focused-ion-beam thinning of frozen-hydrated biological specimens for cryo-electron microscopy. *Nat. Methods* **4**, 215-217.
Marton, L. (1934). Electron microscopy of biological objects. *Nature* **133**, 911.
McIntosh, J. R. (2007). Cellular electron microscopy. *Methods Cell Biol.* **79**, 1-850. Elsevier Science.
Medalia, O. and Geiger, B. (2010). Frontiers of microscopy-based research into cell–matrix adhesions. *Curr. Opin. Cell Biol.* **22**, 659-668.
Medalia, O., Weber, I., Frangakis, A. S., Nicastro, D., Gerisch, G. and Baumeister, W. (2002). Macromolecular architecture in eukaryotic cells visualized by cryoelectron tomography. *Science* **298**, 1209-1213.
Medalia, O., Beck, M., Ecke, M., Weber, I., Neujahr, R., Baumeister, W. and Gerisch, G., (2007). Organization of actin networks in intact filopodia. *Curr. Biol.* **17**, 79-84.
Milazzo, A.-C., Cheng, A., Moeller, A., Lyumkis, D., Jacovetty, E., Polukas, J., Ellisman, M. H., Xuong, N.-H., Carragher, B. and Potter, C. S. (2011). Initial evaluation of a direct detection device detector for single particle cryo-electron microscopy. *J. Struct. Biol.* **176**, 404-408.
Murata, K., Liu, X., Danev, R., Jakana, J., Schmid, M. F., King, J., Nagayama, K. and Chiu, W. (2010). Zernike phase contrast cryo-electron microscopy and tomography for structure determination at nanometer and subnanometer resolutions. *Structure* **18**, 903-912.
Murphy, G. E. and Jensen, G. J. (2007). Electron cryotomography. *Biotechniques* **43**, 413-421, 417 passim.
Narita, A., Mueller, J., Urban, E., Vinzenz, M., Small, J. V. and Maéda, Y. (2012). Direct determination of actin polarity in the cell. *J. Mol. Biol.* **419**, 359-368.
Nicastro, D., Frangakis, A. S., Typke, D. and Baumeister, W. (2000). Cryo-electron tomography of neurospora mitochondria. *J. Struct. Biol.* **129**, 48-56.
Nickell, S., Mihalache, O., Beck, F., Hegerl, R., Korinek, A. and Baumeister, W. (2007a). Structural analysis of the 26S proteasome by cryoelectron tomography. *Biochem. Biophys. Res. Commun.* **353**, 115-120.
Nickell, S., Park, P. S.-H., Baumeister, W. and Palczewski, K. (2007b). Three-dimensional architecture of murine rod outer segments determined by cryoelectron tomography. *J. Cell Biol.* **177**, 917-925.
Ohta, K., Okayama, S., Togo, A. and Nakamura, K.-i. (2014). Three-dimensional organization of the endoplasmic reticulum membrane around the mitochondrial constriction site in mammalian cells revealed by using focused-ion beam tomography. *Microscopy* **63**, i34.
Passarelli, M. K. and Ewing, A. G. (2013). Single-cell imaging mass spectrometry. *Curr. Opin. Chem. Biol.* **17**, 854-859.
Patla, I., Volberg, T., Elad, N., Hirschfeld-Warneken, V., Grashoff, C., Fässler, R., Spatz, J. P., Geiger, B. and Medalia, O. (2010). Dissecting the molecular architecture of integrin adhesion sites by cryo-electron tomography. *Nat. Cell Biol.* **12**, 909-915.
Rigort, A., Bäuerlein, F. J. B., Villa, E., Eibauer, M., Laugks, T., Baumeister, W. and Plitzko, J. M. (2012). Focused ion beam micromachining of eukaryotic cells for cryoelectron tomography. *Proc. Natl. Acad. Sci. USA* **109**, 4449-4454.
Ruskin, R. S., Yu, Z. and Grigorieff, N. (2013). Quantitative characterization of electron detectors for transmission electron microscopy. *J. Struct. Biol.* **184**, 385-393.
Schorb, M. and Briggs, J. A. G. (2014). Correlated cryo-fluorescence and cryo-electron microscopy with high spatial precision and improved sensitivity. *Ultramicroscopy* **143**, 24-32.
Schröder, R. R. (2015). Advances in electron microscopy: a qualitative view of instrumentation development for macromolecular imaging and tomography. *Arch. Biochem. Biophys.* **581**, 25-38.
Schur, F. K. M., Hagen, W. J. H., Rumlová, M., Ruml, T., Müller, B., Kräusslich, H.-G. and Briggs, J. A. G. (2015). Structure of the immature HIV-1 capsid in intact virus particles at 8.8 Å resolution. *Nature* **517**, 505-508.
Shahmoradian, S. H., Galaz-Montoya, J. G., Schmid, M. F., Cong, Y., Ma, B., Spiess, C., Frydman, J., Ludtke, S. J. and Chiu, W. (2013). TRiC's tricks inhibit huntingtin aggregation. *eLife* **2**, e00710.
Small, J. V. (2015). Pushing with actin: from cells to pathogens. *Biochem. Soc. Trans.* **43**, 84-91.
Sorrentino, S., Studt, J.-D., Medalia, O. and Tanuj Sapra, K. (2015). Roll, adhere, spread and contract: structural mechanics of platelet function. *Eur. J. Cell Biol.* **94**, 129-138.
Stauffer, S., Rahman, S. A., de Marco, A., Carlson, L.-A., Glass, B., Oberwinkler, H., Herold, N., Briggs, J. A. G., Müller, B., Grünewald, K. et al. (2014). The nucleocapsid domain of Gag is dispensable for actin incorporation into HIV-1 and for association of viral budding sites with cortical F-actin. *J. Virol.* **88**, 7893-7903.
Stoffler, D., Feja, B., Fahrenkrog, B., Walz, J., Typke, D. and Aebi, U. (2003). Cryo-electron tomography provides novel insights into nuclear pore architecture: implications for nucleocytoplasmic transport. *J. Mol. Biol.* **328**, 119-130.
Svitkina, T. (2010). Imaging cytoskeleton components by electron microscopy. *Methods Mol. Biol.* **586**, 187-206.
von Appen, A., Kosinski, J., Sparks, L., Ori, A., DiGuilio, A. L., Vollmer, B., Mackmull, M.-T., Banterle, N., Parca, L., Kastritis, P. et al. (2015). In situ structural analysis of the human nuclear pore complex. *Nature* **526**, 140-143.
Wagenknecht, T., Hsieh, C. and Marko, M. (2015). Skeletal muscle triad junction ultrastructure by Focused-Ion-Beam milling of muscle and Cryo-Electron Tomography. *Eur. J. Transl. Myol.* **25**, 49-56.
Wang, R., Stone, R. L., Kaelber, J. T., Rochat, R. H., Nick, A. M., Vijayan, K. V., Afshar-Kharghan, V., Schmid, M. F., Dong, J. F., Sood, A. K. et al. (2015). Electron cryotomography reveals ultrastructure alterations in

platelets from patients with ovarian cancer. *Proc. Natl. Acad. Sci. USA* **112**, 14266-14271.

Woodward, C. L., Mendonça, L. M. and Jensen, G. J. (2015). Direct visualization of vaults within intact cells by electron cryo-tomography. *Cell. Mol. Life Sci.* **72**, 3401-3409.

Zhao, X., Norris, S. J. and Liu, J. (2014). Molecular architecture of the bacterial flagellar motor in cells. *Biochemistry* **53**, 4323-4333.

Zuber, B., Chami, M., Houssin, C., Dubochet, J., Griffiths, G. and Daffé, M. (2008). Direct visualization of the outer membrane of mycobacteria and corynebacteria in their native state. *J. Bacteriol.* **190**, 5672-5680.

Journal of Cell Science